Journal of Materials Science and Engineering A 7 (7-8) (2017) 178-187
doi: 10.17265/2161-6213/2017.7-8.002

Electron Microscopy Investigation of FeNi/NrGO Nanocomposite Catalysts for Fuel Cells Application

Warapa Susingrat[1], Thapanee Sarakonsri[1,2], Nutpaphat Jarulertwathana[1], Jaroon Jakmunee[1], Khac Duy Pham[3] and Chung Hoeil[3]

1. Department of Chemistry, Faculty of Science, Chiang Mai University, Chiang Mai 50200, Thailand

2. Material Science Research Center, Faculty of Science, Chiang Mai University, Chiang Mai 50200, Thailand

3. Department of Chemistry and Research Institute for Natural Sciences, Hanyang University, Seoul 133-791, Korea

Abstract: High efficiency but low cost FeNi nanoparticles supported on NG (nitrogen-doped graphene) catalysts for ORR (oxygen reduction reaction) were prepared by electrodeposition method. NG was obtained via thermal annealing of ball milled graphene with melamine. XRD (X-ray diffraction), Raman, and XPS (X-ray photoelectron spectroscopy) analyses showed multiple layers with a low degree of disorder and characteristic of pyridinic-N were a major feature. The deposition of FeNi was carried out potentiostatically with voltage of -7.0 and -6.0 V for 100 s at room temperature. Different concentration of $FeCl_2 \cdot 4H_2O$ and $NiCl_2 \cdot 6H_2O$ in ethylene glycol solution was varied. XRD patterns confirmed FeNi alloy formation and SEM (scanning electron microscopes) images reviewed that 0.025 M FeNi solution achieved spherically dispersed FeNi nanoparticles with diameters of 50-100 nm cover on NG particles and some parts appear as corals shape dendrite cluster. Only spherical particles were observed in other conditions. Average sizes of particle vary without trend. CV analysis shows that catalysts prepared with 0.50 M and at -7.0 V which has the smallest particle sizes, gave higher performance over others and commercial Pt/C catalysts. Therefore, this catalyst is expected to have good performance in ORR.

Key words: Nitrogen-doped graphene, FeNi, electrodeposition method, oxygen reduction reaction.

1. Introduction

The global energy crisis and human-induced climate change have become controversies over the past decade. Carbon dioxide emission has increased rapidly mainly due to increased industrial activities [1]. This leads to the need for alternative energy sources and cleaner means of transportation, to reduce CO_2 emission. Utilization of solar, wind, geothermic, bio-energy and hydrogen is being developed. A zero-emission hydrogen fuel cell is one of the most promising energy sources. Recently, it has been used in the automotive industry. Fuel cells are also suitable for many other applications, such as electrical appliances and portable vehicles, because of their high efficiencies and smaller footprints. Among various types of fuel cells, PEMFC (proton exchange membrane fuel cell) is considered as a promising power source for the next generation portable vehicles, due to its low operating temperature, high energy density and green emission [2, 3]. For the conversion of chemical energy into electricity, PEMFC requires the development of better catalyst, such as Pt-based for the ORR (oxygen reduction reaction). However, pure Pt is not suitable for the ORR because Pt provides two-step pathway of the oxygen reduction. The intermediate product, H_2O_2, can destroy the electrode surface when it is used for a long time [3, 4]. One possible solution is to replace Pt-based catalyst by the non-noble metals—based ones, such as transition metals (Fe, Co, and Ni). FeOOH/reduced graphene oxide hybrids [5] and Fe catalyst supported on nitrogen-functionalized graphene nano-flakes [6] showed good electrochemical catalytic activity for ORR.

Corresponding author: Thapanee Sarakonsri, Ph.D., associated professor, research field: materials chemistry.

Furthermore, the use of carbon-based supports such as carbon black, carbon nanotubes, activated carbons and graphene [2, 5-10] enhanced the catalytic performances of iron (Fe) and nickel (Ni) catalysts. Among these supports, graphene, a 2D single layer sheet of hexagonal carbon atoms, has emerged as a new generation catalyst support because of its high surface area, excellent electrical conductivity, good chemical and environmental stabilities and strong coupling with catalyst nanoparticles. Recently, N-doped carbon which improves ORR activity significantly was proposed [11, 12]. Nitrogen doping increases the basicity of the attached graphitic carbon as a result of the lone pair of electrons of the pyridinic-N species, which stabilizes the carbon against oxidation and facilitates oxygen reduction.

Nowadays, graphene can be prepared by various techniques, such as micromechanical cleavage and exfoliation [13], plasma enhanced chemical vapor deposition [14, 15] and chemical route via reduction of GO (graphene oxide) [16-18]. Among these methods, the chemical oxidations of graphite to form GO and its subsequent reduction to graphene is considered one of the most promising approaches to produce graphene in large volume. However, it was usually carried out using hydrazine as reducing agent [19, 20], which is highly toxic, making great care for a requirement of the GO reduction process. The thermal reduction was chosen in this research because of its low-cost, ease of preparation and effectiveness especially when preparing rGO (reduced graphene oxide) sheets in high quantity [16].

Several methods including microwave [7], chemical reduction [19], mechanical alloying [21], chemical vapor deposition [22] and electrochemical deposition [8] were used to prepare nanostructured FeNi materials. Among these methods, electrodeposition is a simple method of preparation, incurring the low cost and provides good control over particle size and morphology. The FeNi electrocatalysts can be deposited on the surface of functionalized N-doped graphene by chemical reduction of Ni^{2+} and Fe^{2+} ions and directly adsorbed on the N-doped graphene surface. However, there is no report on growing FeNi electrocatalyst on N-doped graphene surface by electrodeposition in the literature.

2. Experimental Setup

2.1 Graphene Nanosheets and Nitogen-Doped Graphene Preparation

GO was prepared first by using the modified Hummers' method [23]. The GO was mashed in mortar for 30 min. The reduction of GO was carried out by thermal annealing with a flow of nitrogen gas and heated to 500 °C at a rate of 3 °C/min. After the temperature maintained for 5 h, the furnace was slowly cooled to room temperature. The obtained graphene (marked as GN) was then balling milled for 3 h. The final product was collected from the crucible directly. The obtained supporter was marked as GN-BM. The N-doped grapheme was prepared by annealing GN-BM and melamine with the mass ratio of 1:5. A mixture was carried out by thermal annealing with a flow of nitrogen and heated to 800 °C at a rate of 5 °C/min. The temperature was maintained for 1 h. The product was marked as NG.

2.2 Preparation of FeNi/Graphene Sheets

The working electrode was prepared by attaching carbon cloth (size 9×6 mm) with titanium foil (size 3×6 mm) by silver paste and dried in an oven at 60 °C for 2-3 h. Afterward, 70 mg of NG was dispersed in the mixture of 47 μL of 5% nafion, 6 μL of distilled water, and 23 μL of isopropanol solutions and sonicated for 30 min. The solution was then dropped onto carbon-cloth substrate and dried in an oven for over 3 h.

NG/carbon-cloth was used as a working electrode, a Pt wire electrode was used as the auxiliary electrode and a Ag/AgCl electrode was used as the reference electrode. The electrolyte for deposition was composed of 0.025 M $FeCl_2 \cdot 4H_2O$ and 0.025 M $NiCl_2 \cdot 6H_2O$ dissolved in ethylene glycol.

Electrodeposition was carried out at room temperature and a constant applied cell voltage of -7.0 V (versus Ag/AgCl) with a deposition time of 100 s. After that, the electrode was rinsed with ethanol and dried in a vacuum oven. The procedure was repeated with the electrolyte concentrations varied to 0.050 M, and with the cell voltage varied to -6.0 V. The names and preparation conditions for all prepared products are shown in Table 1.

2.3 Characterization

All prepared catalysts were firstly characterized by powder X-ray diffraction (XRD, Rigaku MiniFlex 600) for phase identification. The instrument used Cu K_α radiation (λ = 1.5418 Å) operating at 20 kV and 15 mA, with a scanning rate of 0.040/s in the 2θ range of 10-90°. The sample identification was assisted by STOE win XPOW Computer Software (search-match program). The morphology of all products was analyzed by SEM (scanning electron microscopes, JEOL JSM-IT300 and JSM-5910LV), operating at the accelerating voltage of 15-20 kV. Type and percent weight of element were analyzed by EDS (energy dispersive spectroscopy). The morphology and structure of all products were also characterized by TEM (transmission electron microscope, JEOL model JEM-2010), operating at 20 kV. Electrochemically testing by cyclic voltammetric technique was performed. Cyclic voltammetry method was applied to study ORR process. Electrochemical test was performed with a galvanostat/potentiostat. A counter electrode, reference electrode and working electrode were a platinum wire, a Ag/AgCl with saturated KCl solution and the prepared FeNi/graphene catalyst electrode, respectively. The prepared FeNi/graphene electrodes were tested from 1.2 to -0.2 V vs. Ag/AgCl with a scan rate of 20 mV/s. The O_2-saturated 0.025 M $FeCl_2 \cdot 4H_2O$ and $NiCl_2 \cdot 6H_2O$ was used as electrolyte solution. The test temperature of the cell was kept at 25 °C throughout the testing process.

Table 1 Names and conditions for the preparation of the NiFe/Carbon supported products.

Name	Fe-Ni concentration (M)	Applied voltage (V vs. Ag/AgCl)
25FeNi-6V/GN-BM	0.025	-6.0
25FeNi-7V/GN-BM	0.025	-7.0
50FeNi-6V/GN-BM	0.050	-6.0
50FeNi-7V/GN-BM	0.050	-7.0
25FeNi-6V/NG	0.025	-6.0
25FeNi-7V/NG	0.025	-7.0
50FeNi-6V/NG	0.050	-6.0
50FeNi-7V/NG	0.050	-7.0

3. Experimental Results

XRD (X-ray diffraction) patterns obtained from GO, GN-BM, and NG are presented in Fig. 1. It can be seen that the XRD pattern of GO is that of a typical graphite oxide, with the diffraction peak at 2θ = 11.60°, which corresponds to a (001) refection plane (JCPDS file No. 41-1487). After the GO reduction via thermal annealing under nitrogen gas and ball milling, the graphene products (labeled as GN-BM) showed substantially different patterns, with the weak (002) diffraction peak at 2θ = 25.26°. This is reported on the database JCPDS file No. 26-1079. These results confirm that the GO was reduced to GN-BM, but the presence of the (002) diffraction peak in the GN-BM indicated that the synthesized graphene does not exist as a single layer. The GN-BM was then doped with nitrogen (N-doped graphene was prepared by annealing GN-BM and melamine at 800 °C for 1 h with a mass ratio of 1:5). The NG diffraction peak at 2θ = 44°—sign of incorporation of nitrogen in the

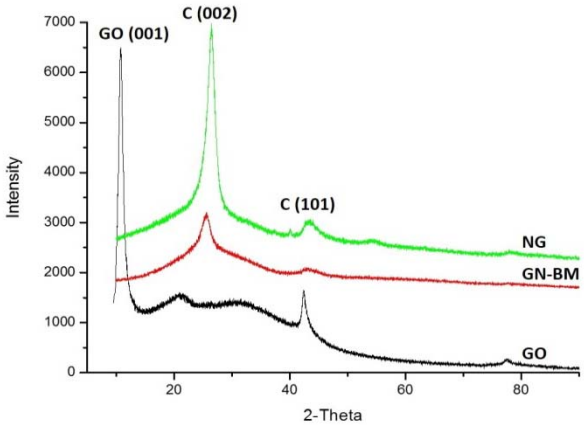

Fig. 1 Powder XRD patterns of GO, GN-BM, and NG.

graphene structure, which suggests the formation of N-doped carbon.

Fig. 2 shows typical analytical data on Raman spectra for GO and GN-BM prepared in this research. Raman spectra provide information about the characterization of structure and quality of carbon materials, particularly the defects, ordered and disordered structures and layers of graphene. The Raman spectra of GO and GN-BM showed two strong peaks at 1,343 and 1,585 cm^{-1}, corresponding to the well-defined D band and G band, respectively. The weak peak at 2,700 cm^{-1} is a second-order of the 2D band. The ratio of I_D/I_G was designed the degree of disorder, such as defects and edges [11, 24, 25]. The I_D/I_G ratios of GO and GN-BM were found to be 0.92 and 0.85 respectively. The lower value of I_D/I_G corresponds to better quality carbon. The higher value of I_D/I_G may be a result of the presence of amorphous carbon and defects in the sample.

XPS (X-ray photoelectron spectroscopy) characterizations were further performed to analyze the elemental composition and nitrogen bonding configurations in NG. As shown in Fig. 3a, the XPS spectrum of 3 visible edges located at 285, 399 and 532 eV corresponded to the characteristic K-shell ionization edges of C, N, and O, respectively. The contents of C, N, and O in NG are represented in Table 2. This could be well-confirmed nitrogen doping of GN-BM was achieved. The high-resolution of C 1s XPS spectra (Fig. 3b) showed one main peak at 285.0 eV corresponding to sp^2-hybridization and small signals at 286.6, 288.2 and 290.0 eV, which were attributed to different C-O bonding configurations. The high resolution N 1s XPS spectra gave five peaks: 398.6, 399.8, 401.0, 401.8 and 403.1 eV (Fig. 3c), corresponding to the characteristic of pyridinic-N, pyrrolic-N, graphitic-N, quaternary-N, and oxide-N, respectively. The relative percentages of N content are summarized in Table 3. Pyridinic-N and pyrrolic-N were located at the edges or vacancies of graphene and bonded to two adjacent carbon atoms, donating aromatic with one/two p-electron and leaving behind the lone pair electrons in sp^2 orbitals [26] . According to the literature, the good performance of electrocatalytic ORR activity can be attributed to pyridinic-N and pyrrolic-N [11].

Fig. 4 shows SEM images of carbon GO, GN-BM, and NG. As shown in Fig. 4b, it could be observed that the GN-BM has smallest sheet size. Fig. 4c shows that the morphology of NG was similar to those of GN-BM.

XRD patterns of 25FeNi/GN-BM on carbon cloth and bare carbon cloth are presented in Fig. 5. The diffraction peak at 26.50° observed in all diffraction patterns of carbon-supported metal was attributed to (002) plane of hexagonal structure to carbon. The characteristic peaks of FeNi alloy (JCPDS file No. 37-474.) were observed at 44.64° and 64.98°, corresponding to the diffraction planes of (110) and

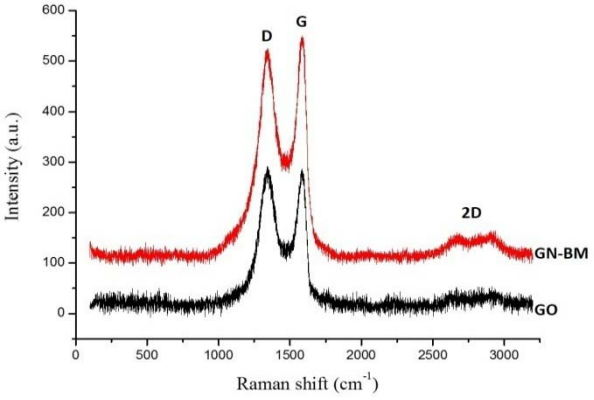

Fig. 2 Raman spectra of GO and BN-BM.

Table 2 Element contents of NG by XPS.

	C 1s	N 1s	O 1s
% atomic	90.21	6.38	3.41
% weight	88.03	7.40	4.57

Table 3 Relative pyridinic-N, pyrrolic-N, graphitic-N, quaternary-N and oxide-N contents and their BE (binding energy) of N 1s peak from XPS.

	% atomic	Binding energy (eV)
Pyridinic-N	52.1	398.6
Pyrrolic-N	19.9	399.8
Graphitic-N	13.9	401.0
Quaternary-N	9.9	401.8
Oxide-N	4.2	403.1

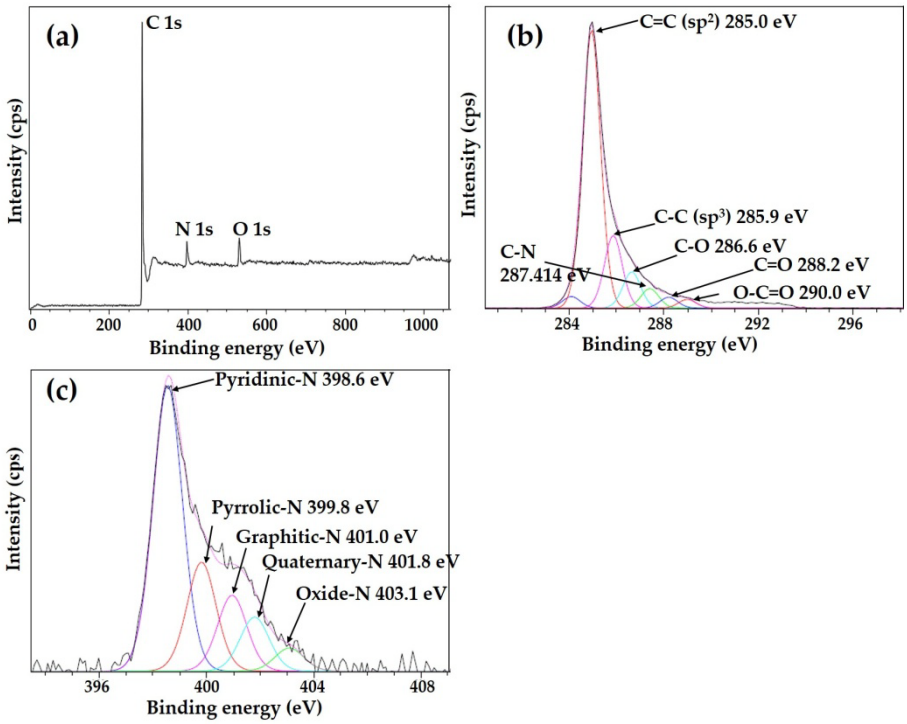

Fig. 3 (a) XPS survey spectrum of NG and high resolution of (b) C 1s and (c) N 1s.

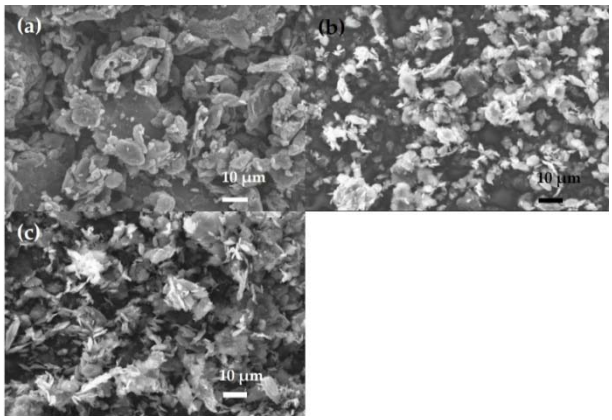

Fig. 4 SEM images of (a) GO, (b) GN-BM and (c) NG.

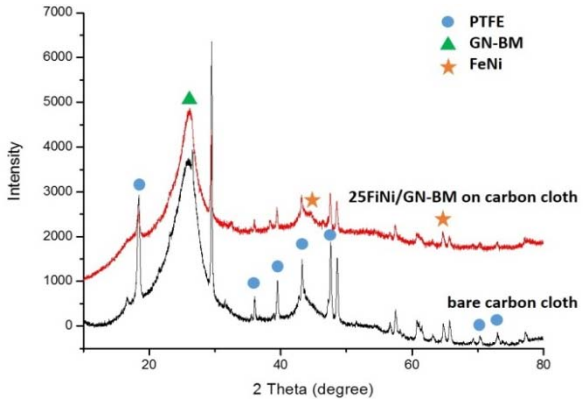

Fig. 5 Powder XRD patterns of bare carbon cloth and 25FeNi/GN-BM on carbon cloth.

(200), respectively. There were also diffraction peaks of poly (tetrafluoroethylene) (PTFE), coated on carbon cloth, at seven diffraction angles: 18.44°, 36.06°, 39.50°, 43.28°, 47.59°, 72.96° and 77.28° [27]. The XRD pattern of 50FeNi/GN-BM on carbon cloth showed the same phases as the 25FeNi/GN-BM on carbon cloth's pattern. Thus, it was confirmed that FeNi alloy could be prepared by the electrodeposition method.

Table 4 shows the EDS results of all prepared FeNi alloy on GN-BM. It confirmed that the FeNi alloy was supported on the GN-BM surface. Moreover, the atomic percentage of Fe and Ni increased as increasing of the precursor concentration. Fig. 6 presents the morphological evolution of FeNi alloy nanoparticles as a function of concentration (0.025 M and 0.050 M FeNi) on GN-BM supported. It can be seen that different morphologies are presented during the different precursor concentrations and deposition voltages. When the $FeCl_2$ and $NiCl_2$ precursors were dissolved and dissociated to Ni^{2+}, Fe^{2+}, and Cl^- ions, the cations could be adsorbed on GN-BM substrate and

Table 4 EDS results for elemental components of FeNi alloy catalysts supported on GN-BM.

Sample name	C (%at)	O (%at)	Fe (%at)	Ni (%at)
25FeNi-6V/GN-BM	14.34	3.42	40.56	41.68
25FeNi-7V/GN-BM	63.58	24.46	8.74	3.22
50FeNi-6V/GN-BM	46.78	25.60	15.99	11.63
50FeNi-7V/GN-BM	59.12	24.56	11.07	5.25

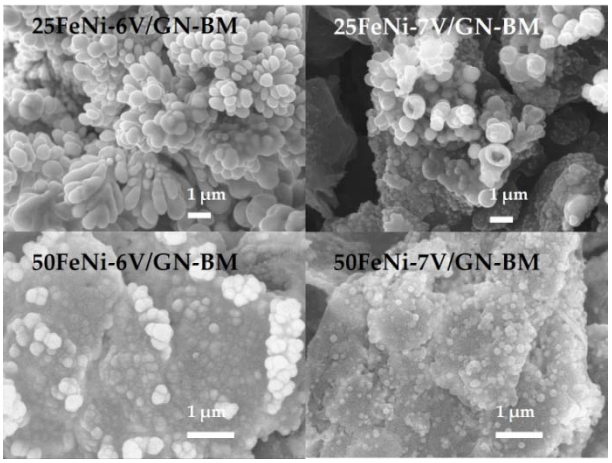

Fig. 6 SEM images of FeNi alloy catalysts supported on GN-BM.

Table 5 EDS results for elemental components of FeNi alloy catalysts supported on NG.

Sample name	C (%at)	O (%at)	N (%at)	Fe (%at)	Ni (%at)
25FeNi-6V/NG	61.11	21.60	1.26	8.64	7.40
25FeNi-7V/NG	67.91	20.00	3.62	4.38	4.09
50FeNi-6V/NG	64.81	17.37	3.36	9.40	5.06
50FeNi-7V/NG	61.91	20.02	2.91	8.88	6.28

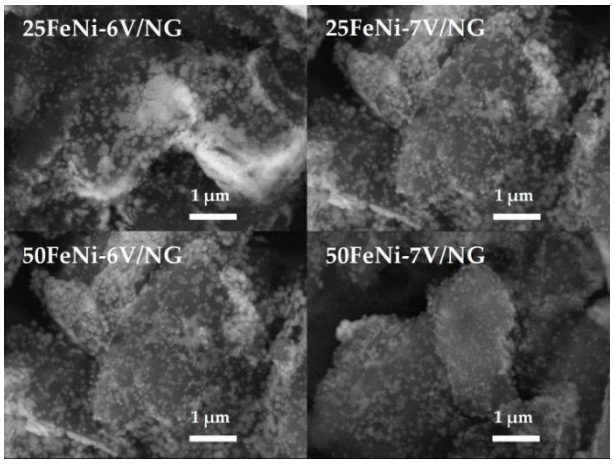

Fig. 7 SEM images of FeNi alloy catalysts supported on NG.

then were reduced to be FeNi alloy. The averages sizes of NiFe particles in 25FeNi-6V/GN-BM, 25FeNi-7V/GN-BM, 50FeNi-6V/GN-BM and 50FeNi-7V/GN-BM were 114, 110, 210 and 122 nm, respectively. It could be seen that an increasing of FeNi concentration from 0.025 M to 0.050 M, with fixed deposition voltage and time, affected the formation of FeNi. The higher concentration of precursors could produce the smaller size of FeNi alloy. The morphological evolution of FeNi alloy nanoparticles as a function of voltages variation (-6 V and -7 V) could also be observed. As the voltage was changed from -6 V to -7 V, the formation of spherical NiFe particles is more favorable than the formation of dendrite FeNi clusters.

Fig. 7 shows the SEM images of products of FeNi alloy on NG supports and their elemental compositions were included in Table 5. The FeNi catalyst was obtained as spherical nanoparticles and dispersed thoroughly on NG surfaces. The quantitative analysis of EDS results confirmed the occurrence of FeNi in the prepared products. The average particle sizes of FeNi in 25FeNi-6V/NG, 25FeNi-7V/NG, 50FeNi-6V/NG and 50FeNi-7V/NG were 86, 88, 82 and 68 nm, respectively. It is obvious that FeNi particles containing in FeNi/NG products were smaller than that containing in FeNi/GN-GM products.

TEM images in Fig. 8 showed that the catalysts consisted of evenly distributed 50-nm-diameter FeNi alloy particles on GN-BM surfaces. The dendrite clusters that appeared in SEM images were not observed in TEM images because the big dendrite clusters were lost during sample preparation. The SAD patterns in the insets of all TEM images showed that the FeNi alloy and carbon contained in all products.

Fig. 9 indicates that there were more catalysts particles on NG supported products than that on GN-BM supported samples. This is a result of higher conductivity of NG which induced Fe^0 and Ni^0 deposition on the NG surfaces. In addition, the more particles of FeNi were produced, the smaller sizes of FeNi particles were obtained on NG.

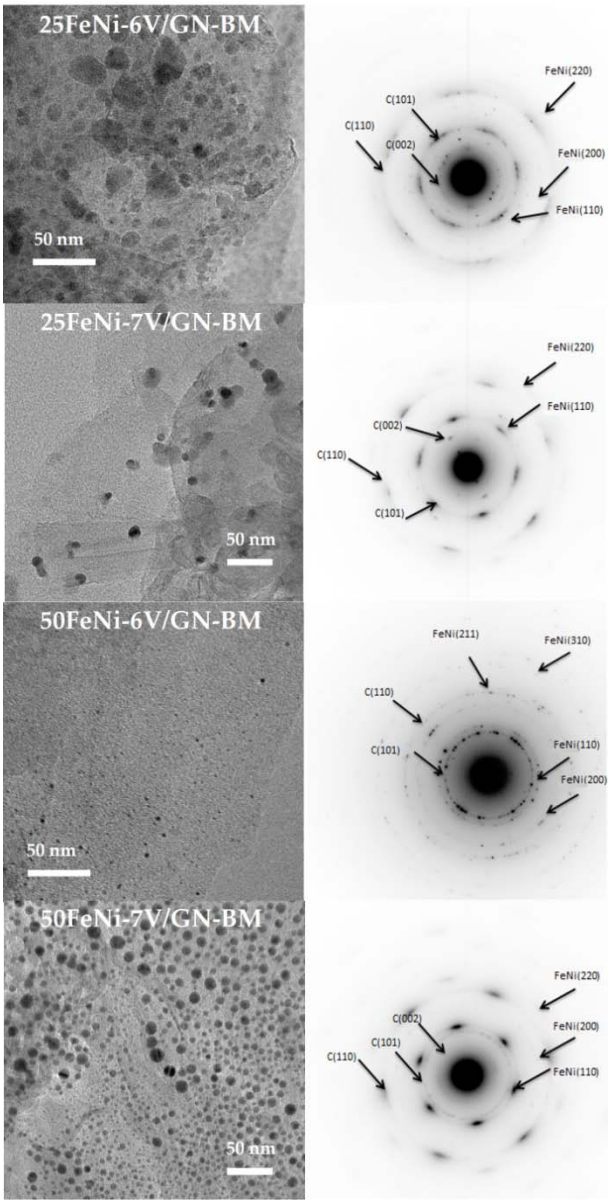

Fig. 8 TEM images with the corresponding SAD patterns of FeNi alloy catalysts supported on GN-BM.

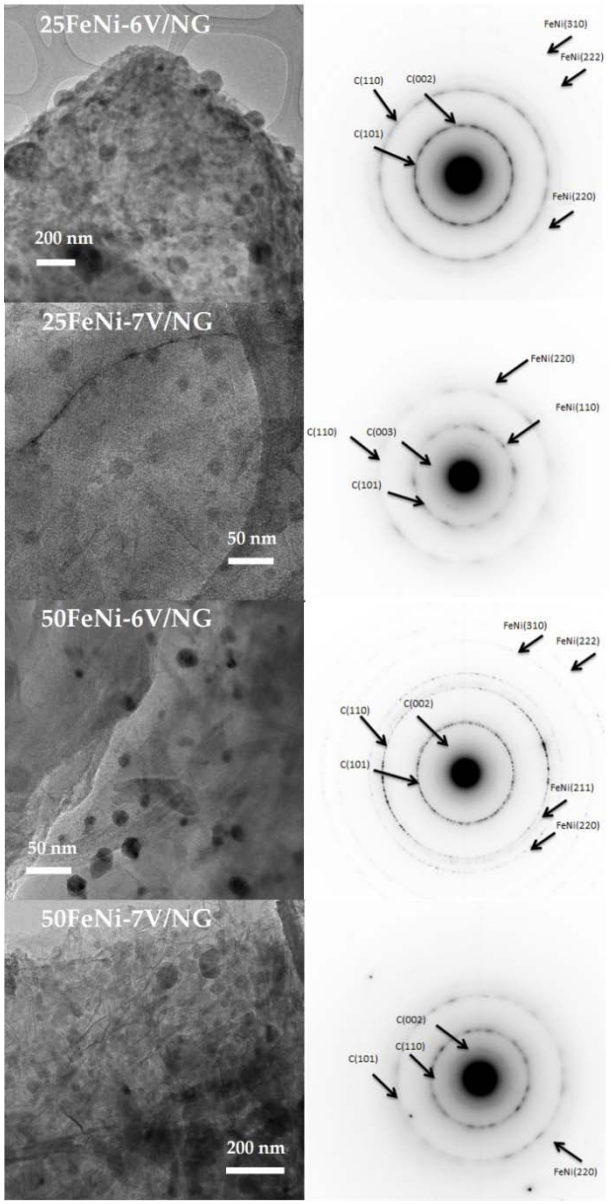

Fig. 9 TEM images with the corresponding SAD patterns of FeNi alloy catalysts supported on NG.

Fig. 10 shows the cyclic voltammograms for ORR at FeNi alloy catalysts supported on GN-BM. The cathodic peaks at around 0.2-0.3 V referred to the ORR. Among these FeNi/GN-BM catalysts, 50FeNi containing higher content of Fe and Ni exhibited more visible ORR peaks than 25FeNi. For the catalysts which were prepared from the same Fe-Ni concentration, the catalysts prepared at the electrodeposition voltage of -7.0 V exhibited the most positive oxygen reduction peak than the others. This result corresponded to the results from SEM and TEM techniques that the smaller sizes and larger surface area of FeNi alloyin 50FeNi-7V/GN-BM provided higher ORR activity.

The cyclic voltammograms for ORR at FeNi alloy catalysts on NG are presented in Fig. 11. The ORR peak of 50FeNi-7V/NG was observed at the most positive oxygen reduction potential at about 0.3 V. This shows the relation between ORR activity and size of FeNi catalysts—the reduction potential increased as decreasing of FeNi particles size. Therefore, 50FeNi-7V/NG exhibited highest catalytic

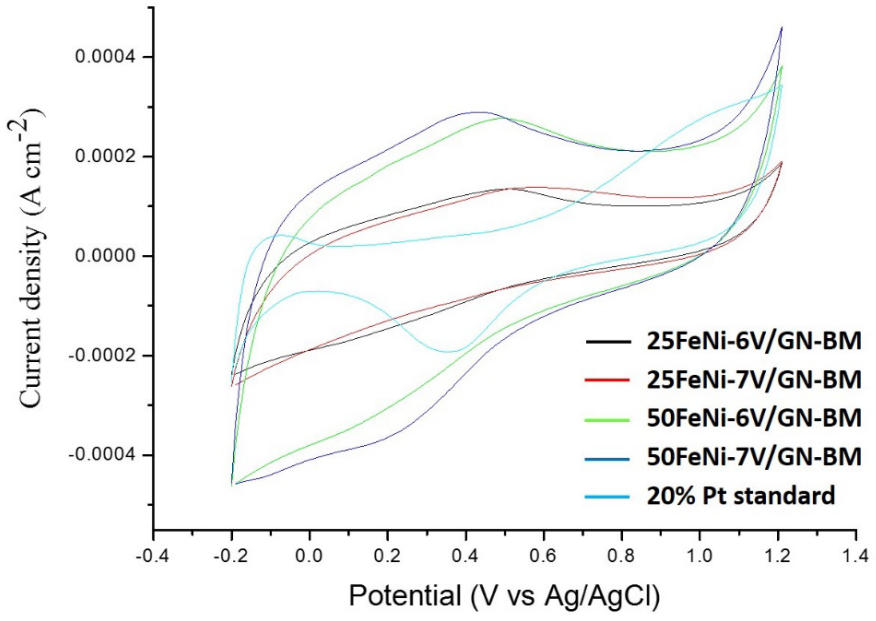

Fig. 10 Typical cyclic voltammograms for ORR obtained at 25FeNi-6V/GN-BM, 25FeNi-7V/GN-BM, 50FeNi-6V/GN-BM, 50FeNi-7V/GN-BM, and commercial 20% Pt catalyst standard from Fuel cell Scientific.

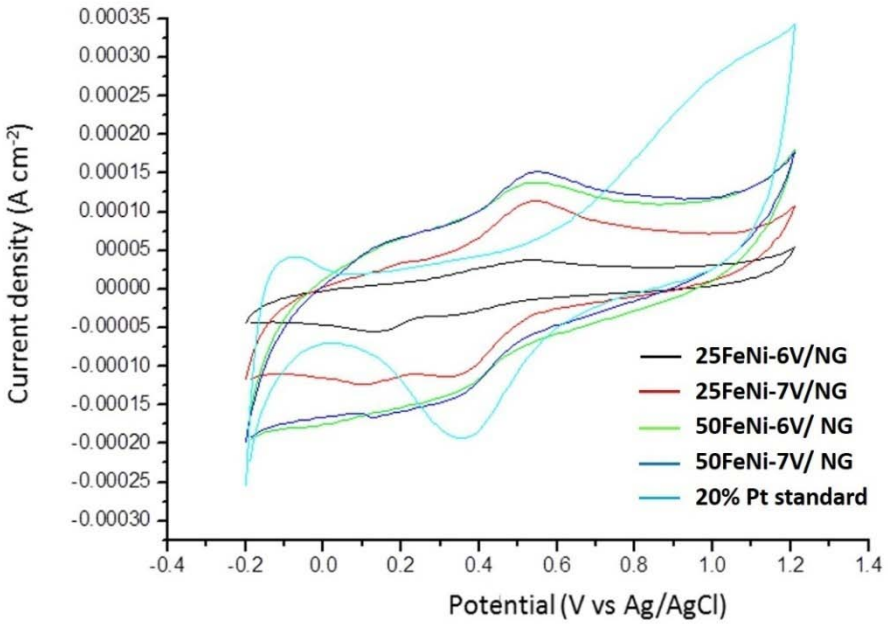

Fig. 11 Typical cyclic voltammograms for ORR obtained at 25FeNi-6V/NG, 25FeNi-7V/ NG, 50FeNi-6V/ NG, 50FeNi-7V/ NGและ and commercial 20% Pt catalyst standard from Fuel cell Scientific.

activity due to its highest surface area of the smallest FeNi particles, the highest content of FeNi alloy and the electrical conductivity of N-doped graphene.

4. Conclusions

In summary, NG which was prepared from the recent work with 6.38% atomic nitrogen exhibited a good support for FeNi alloy. Its high electronic conductivity allowed well dispersion and formation of small FeNi catalyst, leading to high oxygen reduction potential of the prepared product. Therefore, FeNi nanoparticles on NG synthesized via electrodeposition

provided good ORR performance for proton exchange membrane fuel cells.

Acknowledgments

The authors wish to express their appreciation to Materials Science Research Center of Chiang Mai University for the financial support.

References

[1] Zaman, K., and Moemen, M. A. 2017. "Energy Consumption, Carbon Dioxide Emissions and Economic Development: Evaluating Alternative and Plausible Environmental Hypothesis for Sustainable Growth." *Renew. Sustain. Energy Rev.* 74: 1119-30.

[2] An, X., Shin, D., Ocon, J. D., Lee, J. K., Son, Y., and Lee, J. 2014. "Electrocatalytic Oxygen Evolution Reaction at a Feni Composite on a Carbon Nanofiber Matrix in Alkaline Media." *Chinese J. Catal.* 35: 891-5.

[3] Nilekar, A. U., and Mavrikakis, M. 2008. "Improved Oxygen Reduction Reactivity of Platinum Monolayers on Transition Metal Surfaces." *Surf. Sci.* 602: L89-94.

[4] Wang, H., Yuan, X., Li, D., and Gu, X. 2012. "Dendritic Ptco Alloy Nanoparticles as High Performance Oxygen Reduction Catalysts." *J. Colloid Interface Sci.* 384: 105-9.

[5] Lee, S., Cheon, J. Y., Lee, W. J., Kim, S. O., Joo, S. H., and Park, S. 2014. "Production of Novel FeOOH/Reduced Graphene Oxide Hybrids and Their Performance as Oxygen Reduction Reaction Catalysts." *Carbon* 80: 127-4.

[6] Pascone, P.-A., Berk, D., and Meunier, J.-L. 2013. "A Stable and Active Iron Catalyst Supported on Graphene Nano-Flakes for the Oxygen Reduction Reaction in Polymer Electrolyte Membrane Fuel Cells." *Catal. Today* 211: 162-7.

[7] Wen, F., Zhang, F., Xiang, J., Hu, W., Yuan, S., and Liu, Z. 2013. "Microwave Absorption Properties of Multiwalled Carbon Nanotube/Feni Nanopowders as Light-Weight Microwave Absorbers." *J. Magn. Magn. Mater.* 343: 281-5.

[8] Song, S. Q., Liu, Z., Ortega, C. M., Wu, X. S., and Sun, L. 2013. "Electrochemical Study of Ni Deposition on Carbon Microfiber." *Electrochim. Acta* 94: 252-8.

[9] Julkapli, N. M., and Bagheri, S. 2015. "Graphene Supported Heterogeneous Catalysts: An Overview." *Int. J. Hydrogen Energy* 40: 948-79.

[10] Ferrandon, M., Wang, X., Kropf, A. J., Myers, D. J., Wu, G., Johnston, C. M., and Zelenay, P. 2013. "Stability of Iron Species in Heat-Treated Polyaniline–Iron–Carbon Polymer Electrolyte Fuel Cell Cathode Catalysts." *Electrochim. Acta* 110: 282-91.

[11] Sheng, Z.-H., Shao, L., Chen, J.-J., Bao, W.-J., Wang, F.-B., and Xia, X.-H. 2011. "Catalyst-Free Synthesis of Nitrogen-Doped Graphene via Thermal Annealing Graphite Oxide with Melamine and Its Excellent Electrocatalysis." *ACS Nano* 5: 4350-8.

[12] Ma, Y., Wang, H., Key, J., Linkov, V., Ji, S., Mao, X., Wang, Q., and Wang, R. 2014. "Ultrafine Iron Oxide Nanoparticles Supported on N-Doped Carbon Black as an Oxygen Reduction Reaction Catalyst." *Int. J. Hydrogen Energy* 39: 14777-82.

[13] Allen, M. J., Tung, V. C., and Kaner, R. B. "Honeycomb Carbon: A Review of Graphene." *Chem. Rev.* 110: 132-45.

[14] Wang, J. J., Zhu, M. Y., Outlaw, R. A., Zhao, X., Manos, D. M., and Holloway, B. C. 2004. "Free-Standing Subnanometer Graphite Sheets." *Appl. Phys. Lett.* 85: 1264-7.

[15] Wang, J., Zhu, M., Outlaw, R. A., Zhao, X., Manos, D. M., and Holloway, B. C. 2004. "Synthesis of Carbon Nanosheets by Inductively Coupled Radio-Frequency Plasma Enhanced Chemical Vapor Deposition." *Carbon* 42: 2867-72.

[16] Lian, P., Zhu, X., Liang, S., Li, Z., Yang, W., and Wang, H. 2010. "Large Reversible Capacity of High Quality Graphene Sheets as an Anode Material for Lithium-Ion Batteries." *Electrochim. Acta* 55: 3909-14.

[17] Wang, G., Wang, B., Wang, X., Park, J., Dou, S., Ahn, H., and Kim, K. 2009. "Sn/Graphene Nanocomposite with 3D Architecture for Enhanced Reversible Lithium Storage in Lithium Ion Batteries." *J. Mater. Chem.* 19: 8378-84.

[18] Yue, W., Yang, S., Ren, Y., and Yang, X. 2003. "In Situ Growth of Sn, SnO on Graphene Nanosheets and Their Application as Anode Materials for Lithium-Ion Batteries." *Electrochim. Acta* 92: 412-20.

[19] Stankovich, S. et al. 2007. "Synthesis of Graphene-Based Nanosheets via Chemical Reduction of Exfoliated Graphite Oxide." *Carbon N. Y.* 45: 1558-65.

[20] Ul Hasan, K., Sandberg, M., Nur, O., and Willander, M. 2011. "Polycation Stabilization of Graphene Suspensions." *Nanoscale Res. Lett.* 6: 493.

[21] Guittoum, A. et al. 2008. "X-Ray Diffraction, Microstructure, Mössbauer and Magnetization Studies of Nanostructured Fe50Ni50 Alloy Prepared by Mechanical Alloying." *J. Magn. Magn. Mater.* 320: 1385-92.

[22] Yan, W., Wang, D., and Botte, G. G. 2012. "Electrochemical Decomposition of Urea with Ni-Based Catalysts." *Appl. Catal. B Environ.* 127: 221-6.

[23] Wang, S. J., X., and Chang, C.-T. 2014. "Preparation and Characterization of Graphene Oxide." *J. Nanomater* 6.

[24] Yan, Z., and Barron, A. R. 2007. "Characterization of Graphene by Raman Spectroscopy." Accessed July 15,

2017. http://cnx.org/contents/8GImxcKk@2/Characterization-of-Graphene-b.

[25] Cai, D., Wang, S., Lian, P., Zhu, X., Li, D., Yang, W., and Wang, H. 2013. "Superhigh Capacity and Rate Capability of High-Level Nitrogen-Doped Graphene Sheets as Anode Materials for Lithium-Ion Batteries." *Electrochim. Acta* 90: 492-7.

[26] Li, M., Zhang, L., Xu, Q., Niu, J., and Xia, Z. 2014. "N-Doped Graphene as Catalysts for Oxygen Reduction and Oxygen Evolution Reactions: Theoretical Considerations." *J. Catal*. 314: 66-72.

[27] Shulga, Y. M., Vasilets, V. N., Kiryukhin, D. P., Voylov, D. N., and Sokolov, A. P. 2015. "Polymer Composites Prepared by Low-Temperature Post-irradiation Polymerization of C_2F_4 in the Presence of Graphene-Like Material: Synthesis and Characterization." *RSC Adv*. 5: 9865-74.